

Disordered and ordered C₂₈ solids

Jeongnim Kim

Department of Physics, The Ohio State University, Columbus, Ohio 43210

Giulia Galli

Institut Romand de Recherche Numérique en Physique des Matériaux (IRRMA), Ecublens, 1015 Lausanne, Switzerland

John W. Wilkins

Department of Physics, The Ohio State University, Columbus, Ohio 43210

Andrew Canning^{a)}

CRAY Research, PSE, EPFL, 1015 Lausanne, Switzerland

(Received 13 June 1997; accepted 5 November 1997)

Using tight-binding molecular dynamics, we have performed computer experiments to mimic the gas phase growth of a disordered solid composed of C₂₈ fullerenes. The growth has been simulated by repeated low energy collisions of molecules coming from random directions. The resulting solid is composed of undamaged C₂₈ cages, with most fullerenes being three- and four-fold coordinated, similar to C atoms in amorphous materials. The system contains a high percentage of distorted *sp*² C sites and only a small proportion of *sp*³ sites. These results help clarify the structure of disordered films obtained experimentally by small fullerene deposition on surfaces. Furthermore, we have compared the properties of the disordered C₂₈ solid (*a*-C₂₈) with those of ordered C₂₈ solids. We have found that the energy of *a*-C₂₈ is close to that of hyperdiamond (0.1 eV/atom higher) and differs by a few meV from that of other ordered structures, such as 2D-hypergraphite, hexagonal and clathrate solids. This indicates that in condensed phases C₂₈ molecules can act as carbon superatoms, while showing more bonding flexibility than C atoms; in particular the capability of acting as six-fold coordinated building blocks of hexagonal solids, which are as stable as *a*-C₂₈.

© 1998 American Institute of Physics. [S0021-9606(98)52006-5]

I. INTRODUCTION

A growing community of physicists, chemists and material scientists have recently devoted a significant effort to studying and controlling the behavior of small clusters, the main goal being the synthesis of new materials^{1,2} with clusters as building blocks. Since the experimental discovery³ of C₆₀, many investigations on cluster-assembled solids have focused on fullerenes, and most of them have concentrated on the C₆₀ molecule and larger cages.⁴ At present, only a few investigations of nanostructured materials made of fullerenes smaller than C₆₀ have appeared in the literature.^{2,5-11}

Amongst fullerenes with less than 60 atoms, the C₂₈ molecule is one of the most studied.¹²⁻¹⁴ This cluster is believed to be the smallest cage created in the photofragmentation¹² of C₆₀ by loss of C₂, as well as being the smallest fullerene produced in considerable amounts in the laser vaporization of graphite.¹³ The structure of the isolated cluster was first proposed by Kroto,¹⁴ who suggested that C₂₈ should be a cage, chemically very reactive, with four preferred active sites (which we call *A* sites). Based on a series of experiments on laser vapourization of graphite in the presence of transition metals, Guo *et al.*¹³ proposed that it should be possible to stabilize an arrangement of C₂₈ cages

in a diamond lattice, with each molecule bonded together at the four *A* sites. This system is usually referred to as hyperdiamond. Since the conjecture of Ref. 13, several theoretical studies of hyperdiamond have appeared in the literature.⁷⁻¹⁰ However the issues of growth, stability and chemical bonding of other C₂₈ crystalline forms, as well as of disordered C₂₈ solids have not yet been addressed in detail.

Indirect information about disordered C₂₈ solids can be inferred from low energy cluster beam deposition experiments (LECBD) of small fullerenes (C_{*n*}, *n*=20-32) on nonmetallic surfaces.^{5,6} These experiments suggest that the deposition of small fullerenes can produce thin films retaining the bonding properties of the incident clusters. Since small cages contain *sp*³-like sites with a dangling bond, this memory effect might permit the synthesis of amorphous diamond, i.e., of a disordered carbon solid containing a large proportion of *sp*³ diamond-like sites. However the interpretation of Raman and energy loss spectra is controversial and inconclusive about whether the deposited films contain small fullerene cages or a diamond-like network.⁶

In this paper we present a study of the gas phase growth of C₂₈ solids, and a comparative analysis of ordered and disordered C₂₈ assembled structures, focusing on their bonding properties. We studied the growth of an amorphous phase, *a*-C₂₈, by performing molecular dynamics simulations based on a tight-binding Hamiltonian¹⁶ and using a

^{a)}Present address: NERSC, Lawrence Berkeley Laboratory, Berkeley, California 94720.

linear scaling method.^{17,18} The system was grown by repeated low energy collisions of fullerenes coming from random directions. Our results show that similarly to thin films of C₂₈'s deposited on surfaces,¹¹ C₂₈ molecules are almost defect-free building blocks of *a*-C₂₈, with the majority of cages being three- and four-fold coordinated, similar to carbon atoms in amorphous systems. The cohesive energy of *a*-C₂₈ is close to that of hyperdiamond (about 0.1 eV/atom higher) and of a two-dimensional network of C₂₈'s, with the molecule centers of mass occupying the lattice site of graphite (2D-hypergraphite). The cohesive energy of *a*-C₂₈ is a few meV lower than that of other ordered structures, such as hexagonal and clathrate structures. This indicates that the computer generated disordered system is a fairly stable candidate for a gas phase grown C₂₈ solid, although several different packing and bonding arrangements of the C₂₈ molecule in the condensed phase have similar cohesive energies.

The rest of the paper is organized as follows: in Sec. II we explain the methodology used in our simulations; we then present results for disordered and ordered C₂₈ solids in Sec. III, and give our conclusions in Sec. IV.

II. METHOD

In this section we summarize the key features of quantum simulations based on linear scaling approaches.¹⁸ We then discuss the accuracy of the tight-binding Hamiltonian¹⁶ that we chose to describe C₂₈ systems, by comparing results for the monomer, dimer and hyperdiamond obtained both at the tight-binding (TB) and the local density functional (LDA) level. Finally, we give an account of the simulation procedure used to grow an amorphous structure in the gas phase.

A. Quantum simulations using a linear scaling method

In our study we performed molecular dynamics (MD) simulations in which at each step the forces (F_I) acting on ions are determined by computing the gradient of the total energy (E) of electrons in the field of ions, with respect to the ionic degrees of freedom, as described within a semi-empirical tight-binding formulation:

$$F_I = -\nabla_I E[\{\mathbf{R}_I\}]. \quad (1)$$

Here $\{\mathbf{R}_I\}$ represent ionic coordinates and

$$E = E_{BS} + \sum_{LL'} V_R(|\mathbf{R}_L - \mathbf{R}_{L'}|). \quad (2)$$

The term V_R is a repulsive two body potential derived from fits to first-principles calculations for ordered carbon solids.¹⁶ In standard approaches the band structure term E_{BS} is written as

$$E_{BS} = \sum_i^{N/2} f_i \langle \psi_i | \hat{H} | \psi_i \rangle, \quad (3)$$

where \hat{H} is a TB Hamiltonian, derived for carbon systems by Xu *et al.*¹⁶ and ψ_i are its eigenstates, i.e., the single particle wave functions minimizing the functional E_{BS} . The total

number of electrons is N and the total number of single particle states is $N/2$, assuming double occupancy for each state ($f_i = 2$).

The direct diagonalization of \hat{H} needed at each step of a MD simulation requires a number of operations scaling as the third power of N , i.e., a computational workload of order N^3 ($O(N^3)$ -scaling). This limits the number of atoms that can be studied in conventional TB-MD simulations to less than a few hundreds using workstations and to less than 1000, when using powerful supercomputers. In order to extend quantum MD studies to larger systems and thus to a broader class of problems, many so called $O(N)$ methods have been introduced in recent years,¹⁸ $O(N)$ meaning that their computational cost grows linearly with the system size. Some of these approaches are based on an orbital formulation of the electronic properties whereas others are based on the calculation of the Green's function, density matrix or the density. In this work we chose to evaluate the energy E_{BS} using an orbital based $O(N)$ method,¹⁷ which allows us to simulate using workstation systems containing about 800-1000 atoms for tens of picoseconds.

A key point of $O(N)$ methods is the evaluation of total energy and forces without computing the eigenvalues and eigenstates of \hat{H} . This evaluation is accomplished by dividing the full system into subsystems and then defining electronic orbitals which are localized in the subsystems. Schrödinger-type equations are then iteratively solved for these localized degrees of freedom. The subsystems are overlapping portions of the full system, which we call localization regions. The important point is that the extension of a localization region depends on the physical and chemical properties of the system but not on the entire volume of the system. The size of a localization region is the parameter controlling the accuracy of the calculation. Using localized functions is necessary but in general not sufficient to achieve $O(N)$ scaling. Another key ingredient is the definition of an appropriate energy functional whose minimization requires neither explicit orthonormalization of electronic orbitals, nor the inversion of an overlap matrix (\mathbf{S}) between single particle wave functions. Such a functional is in general different from the functional E_{BS} of Eq. (2), but it has the same absolute minimum.

In our calculations, at each MD step we minimized the generalized functional

$$E_{GBS}[\{\phi\}, \mu, M] = 2 \sum_{ij=1}^M (2\delta_{ij} - S_{ij}) \langle \phi_j | \hat{H} - \mu | \phi_i \rangle + \mu N \quad (4)$$

with respect to electronic orbitals $\{\phi\}$, which are localized in appropriate regions of real space, the localization regions. We call these orbitals localized orbitals (LOs). The matrix $(2\mathbf{I} - \mathbf{S})$ is the truncated series expansion of \mathbf{S}^{-1} to the first order, with $S_{ij} = \langle \phi_i | \phi_j \rangle$. The functional (4) depends on M orbitals—with M in general larger than the number of occupied electronic states $N/2$ —, and on a global variable μ , determining the appropriate filling of the LOs.

By definition, the orbitals $\{\phi\}$ have finite components only inside the localization regions (LRs) and are zero out-

side. While the number and centers of LRs are arbitrary, we chose a number of LRs equal to the number of atoms, each centered at an atomic site (I). A localized orbital is then specified by its localization region, i.e., the region of space where it has finite-components, and its center, i.e., the center of the LR. We considered three localized orbitals per atomic site, amounting to a total of $M=3N/4$ localized orbitals in our calculation, and LRs extending up to third neighbors. The localized orbital $|\phi_i\rangle$, whose center is the I th atom, is expressed as

$$|\phi_i\rangle = \sum_{J \in \{LR_I\}} \sum_l C_{Jl}^i |\alpha_{Jl}\rangle, \quad (5)$$

where $|\alpha_{Jl}\rangle$'s are the atomic basis functions of the atom J and the index l indicates the atomic components (s, p_x, p_y , or p_z). Here $\{LR_I\}$ indicate the set of atoms belonging to the localization region of the orbital $|\phi_i\rangle$. The generalized functional of Eq. (4) was minimized using a conjugate gradient (CG) procedure, where the derivative

$$\frac{\partial E_{GBS}}{\partial \phi_i} = 4 \sum_j^M [(H - \mu) |\phi_j\rangle (2\delta_{ji} - S_{ji}) - |\phi_j\rangle \langle \phi_j | (H - \mu) | \phi_i \rangle] \quad (6)$$

is evaluated at each iterative step. During the functional minimization μ is varied until the total charge of the system equals N ; thus when convergence is achieved, i.e., the ground state is attained, the value of μ coincides with that of the electronic chemical potential. The variation of μ during the minimization procedure allows for long-range charge transfers in the minimization process, irrespective of the extent of the LRs. Therefore, the variation of μ during the minimization procedure helps avoiding traps at local minima, which were found in minimizations using a number of LOs equal to the number of electronic states.¹⁷

During molecular dynamics runs, in order to prevent unphysical charge transfers between neighboring atoms, we added to the Hamiltonian \hat{H} a Hubbard-type term¹⁶ $H_U = U \sum_I (q_I - q_I^0)^2$, where q_I is the Mulliken population at atomic site I , q_I^0 equals the valence atomic charge and U is a constant. The Mulliken population is given by $q_I = 2 \sum_{ij} (2\delta_{ij} - S_{ij}) \langle \phi_i | R_I \rangle \langle R_I | \phi_j \rangle$, where $\langle \phi_i | R_I \rangle$ indicates the projection of the localized orbital ϕ_i onto the localization region associated to atom I . In the presence of a Hubbard like term, the line minimization required in a CG procedure amounts to the minimization of a polynomial of eighth degree in the variation of the wave function along the conjugate direction. In our calculations, we performed an exact line minimization by evaluating the coefficients of the polynomial.

B. Tight-binding and first-principles results for simple C_{28} systems

The TB-Hamiltonian proposed by Xu *et al.*¹⁶ has been successfully used to study a variety of carbon systems, including fullerenes.¹⁹ In order to test the validity of both the TB-Hamiltonian and the $O(N)$ method described above to study C_{28} systems, we compared the results for the structure

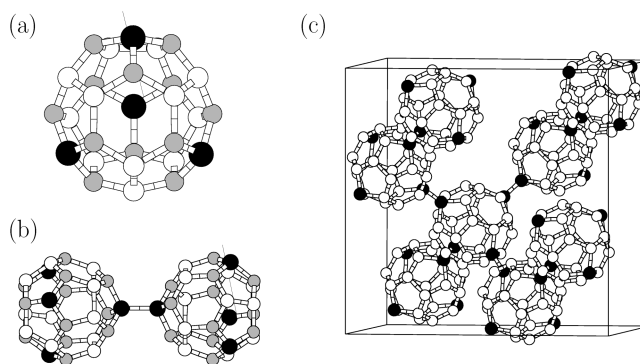


FIG. 1. (a) The C_{28} molecule, (b) the C_{28} dimer and (c) hyperdiamond. In (a) and (b) black, gray and white spheres indicate A , B and C sites, respectively. In (c) black spheres indicate A sites and white spheres both B and C sites (see text).

and bonding of the C_{28} monomer, dimer and hyperdiamond (see Fig. 1) obtained by performing first-principles and $O(N)$ -TB calculations. As discussed in detail below, the agreement between *ab initio* and $O(N)$ -TB results is extremely good.

The LDA calculations for the monomer and the dimer were carried out within the pseudopotential-plane-wave formalism,²⁰ using Troullier-Martins pseudopotentials²¹ and a kinetic energy cutoff of 30 to 44 Ry (to check for convergence). We used supercells of dimensions $(15.9 \text{ \AA})^3$ and $(15.9 \text{ \AA} \times 15.9 \text{ \AA} \times 23.8 \text{ \AA})$ for the monomer and the dimer, respectively. Since the C_{28} molecule is Jahn-Teller distorted and polarization effects can be important, we checked for convergence of total energy with respect to cell size and found that in a cell of $(15.9 \text{ \AA})^3$ this energy was converged up to 0.005 eV.

The C_{28} monomer, shown in Fig. 1(a), is composed of 12 pentagons and 4 hexagons; atoms at an apex where three pentagons meet are denoted as A sites; atoms on the hexagons are denoted as B sites if bonded to A sites, and C sites otherwise. The C_{28} molecule has 12 A - B , 24 B - C and 6 C - C bonds; the bond distances obtained within LDA and $O(N)$ -TB, reported in Table I, are in satisfactory agreement. We note that the molecule has C_1 and not T_d symmetry, due to a Jahn-Teller distortion.

In order to determine stable configurations of the C_{28} dimer, we performed $O(N)$ -TB-MD simulations of low energy collisions between two C_{28} molecules. These will be described in detail in Sec. III. We found that stable configurations are formed by two C_{28} molecules connected by only a single bond. We considered in particular three cases involving A and C atoms as bonding sites, since these are the most reactive sites.¹¹ Within both LDA and $O(N)$ -TB we found that the most stable configuration is an A - A bonded dimer [shown in Fig. 1(b)]; A - C and C - C bonded configurations (see Table I) have cohesive energies about 0.8 eV lower than that of the A - A bonded dimer. We note that ionic positions of both the monomer and the dimer were fully optimized in our calculations, and the rotational configuration of the dimer was the same for both $O(N)$ -TB and LDA calculations.

Figure 1(c) displays an eight-cluster-hyperdiamond supercell showing one four-fold coordinated molecule. In hy-

TABLE I. Comparison between properties of the C_{28} monomer (M) and dimer (D) obtained from first-principles density functional calculations in the local density approximation (LDA) and semiempirical linear scaling calculations (O(N)-TB, see text). The C_{28} monomer is composed of 12 pentagons and 4 hexagons; we denote atoms at an apex where three pentagons meet as A sites; atoms on the hexagons as B sites if bonded to A sites, and C sites otherwise. The C_{28} molecule has 12 A - B , 24 B - C and 6 C - C bonds. The cohesive energy of the dimer is $E_{\text{coh}} = (E^D - 2 \cdot E^M)$, where E^D and E^M are the total energies of D and M , respectively.

C_{28} monomer	O(N)-TB	LDA
A - B bond length (\AA)	1.44–1.46	1.42–1.45
B - C bond length (\AA)	1.40–1.44	1.40–1.44
C - C bond length (\AA)	1.47–1.55	1.46–1.57
C_{28} dimer	O(N)-TB	LDA
A - A bonded R_{eq} (\AA)	1.54	1.51
A - C bonded R_{eq} (\AA)	1.46	1.51
C - C bonded R_{eq} (\AA)	1.50	1.53
A - A bonded E_{coh} (eV)	3.02	3.15
A - C bonded E_{coh} (eV)	2.13	2.48
C - C bonded E_{coh} (eV)	2.24	2.48

perdiamond, the centers of mass of C_{28} molecules are placed on diamond lattice sites and the molecules are bonded together at A sites. The cohesive energy of hyperdiamond, given with respect to the cohesive energy of diamond, is 0.65 and 0.74 eV/atom in O(N)-TB and LDA calculations, respectively; the C_{28} - C_{28} bond lengths and the solid lattice constants are 1.52 and 1.54 \AA , 15.85 and 15.78 \AA , within O(N)-TB and LDA, respectively. This shows again a good agreement between *ab initio* and semi-empirical results. In the O(N)-TB calculation for hyperdiamond both the lattice constant and the atomic positions were optimized. Calculations at the $\mathbf{k}=(0,0,0)$ point of supercells containing 8 and 64 C_{28} 's gave almost identical results for the structural properties of hyperdiamond. The LDA results for hyperdiamond are taken from Ref. 9, where the authors tried three different geometries of the C_{28} cluster composing the solid: the optimized Hartree-Fock geometry, the optimized T_d LDA geometry²² and the optimized LDA geometry of $C_{28}H_4$. The solid structure optimized starting from the $C_{28}H_4$ cluster geometry was found to have the lowest energy. Further relaxation¹⁰ of the cluster geometry within the solid improved very little the total energy per atom (0.01 eV). This is in agreement with O(N)-TB results showing that the optimized geometry of C_{28} in the solid is Jahn-Teller stable, having a symmetry close to T_d . The results of Ref. 9 are in good agreement with those by Bylander and Kleinman⁸ and of Adams *et al.*⁷

C. Collision experiments to grow an amorphous phase

As mentioned in the Introduction, we simulated the growth of an amorphous phase (a - C_{28}) by repeated low energy collisions of fullerenes coming from random directions. In this way we eliminated any effect coming from the presence of a surface in e.g., deposition experiments,¹¹ and could study the bonding properties of a genuine disordered C_{28}

solid. We performed collisions of molecules in pairs so as to preserve the center of mass of the whole system throughout the simulation.

After each collision, heat was removed from the system using a Nose thermostat²³ and then constant temperature MD runs were performed, to keep the system at room temperature. This procedure was preferred to the melting-quenching procedure often used to generate an amorphous structure, where a solid is melted and then the resulting liquid is quenched to low temperature. There are two reasons for this. First, collision computer experiments can mimic deposition processes performed in real experiments. Secondly, *inter*-fullerene bonds are covalent bonds which can be as strong as *intra*-fullerene bonds (see Table I). Therefore the melting of a solid C_{28} structure, e.g., hyperdiamond, will break both *inter*- and *intra*-fullerene bonds and thus induce the breaking apart of the cages.

The O(N)-TB method is particularly well suited to MD simulations in which the number of particles is varied during the run. An extra-particle can be added to a N_c -particles system, at a distance where it does not interact with any of the N_c particles, because of the localization constraints imposed on the electronic orbitals. Thus the set of LO's minimizing the total energy of the (N_c+1)-particle system is initially given by the union of the sets of LOs $\{\phi\}$'s minimizing respectively the E_{GBS} of the N_c and that of the extra-particle systems. A subsequent gradual approach of an extra-particle to the N_c particle system only weakly perturbs its electronic ground state. Therefore the minimization of the TB-Hamiltonian for the (N_c+1)-particle system takes only a small number of steps, i.e., much smaller than any optimization from scratch of the energy of the (N_c+1)-particle system. In our calculation, we could use the same number of CG iterations (20) at each step of the simulation.

We first studied collisions of two C_{28} fullerenes at different incident kinetic energies ($E_i=5, 10, 20, 30$ eV/cluster) and for different cluster orientations, in order to establish an impact regime in which the clusters form bonds without changing their topology. We found the threshold for two clusters to bond at $E_i=5$ eV, and that the topology of the cluster was preserved up to 20 eV. On the other hand, for some orientations at $E_i=30$ eV the C_{28} cages can open and a cage-like C_{56} cluster can be formed. Different orientations of the two incident clusters were tested and the lowest energy of the dimer $(C_{28})_2$ at zero temperature was found for the configuration where two active (A) sites were facing each other.

These results are very different from those of an amorphous system similarly grown by C_{24} fullerene collisions. In collision computer experiments involving C_{24} 's we found that the energy threshold to form intercluster bonds is 20 eV and that the reactions open up the cage, destroying any resemblance to the incident clusters. Even at 20 eV, the final structure is very sensitive to the orientation of two colliding clusters with both open and closed cages formed at the end of a collision. We conclude that contrary to C_{28} , the C_{24} cluster is much less stable to collisions and the formation of an amorphous system composed of C_{24} fullerenes as building blocks is unlikely.

The growth of a - C_{28} was performed at incident kinetic

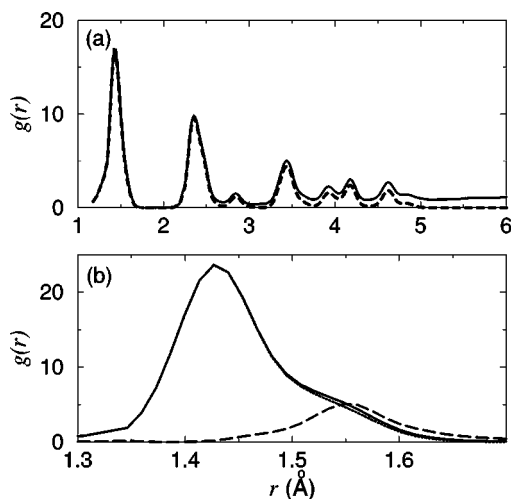


FIG. 2. (a) Particle-particle correlation function of all carbon sites of the amorphous C_{28} solid ($g_{CC}(r)$, solid line), and of those sites involved only in *intra*-clusters bonds ($g_{CC}^{intra}(r)$, dashed line). The data have been convoluted with Gaussians, following the procedure suggested in Ref. 25. We considered Gaussian widths corresponding to a maximum wave vector of 50 \AA^{-1} , which could possibly be attained experimentally, in, e.g., x-ray synchrotron radiation investigations. (b) First peak of $g_{CC}(r)$ (solid line), compared with those of $g_{CC}^{intra}(r)$ (dotted line) and of the correlation function for all atoms taking part in *inter*-cluster bonds ($g_{CC}^{inter}(r)$, dashed line). Here we used Gaussian widths corresponding to a maximum wave vector of 90 \AA^{-1} , in order to make visible the shoulder after the first sharp peak, which would be washed out for smaller wave vectors. The function $g_{CC}^{inter}(r)$ has been arbitrarily scaled in order to be clearly visible on the same scale as the other correlation functions.

energy of 20 eV per cluster. After each collision, the kinetic and potential energy of the system were monitored to establish when the system reached equilibrium. Then the system was cooled down to room temperature with a Nosé thermostat, and finally equilibrated at room temperature before starting another collision. A common time step ($\Delta t = 10$ a.u.) for the integration of the equations of motion was used during the equilibration runs as well as during the collision processes. After growing a supercluster in the gas phase, we performed simulations with periodic boundary conditions in order to minimize the number of dangling bonds and thus surface effects. We then optimized the volume of the system using a damped Andersen dynamics,²⁴ by requiring that the pressure acting on the MD cell vanishes. The integrated simulation time to prepare the amorphous phase of C_{28} is about 50 ps.

III. DISORDERED AND ORDERED C_{28} SOLIDS

The disordered solid grown in our computer simulations is characterized by defect-free fullerenes which retained their topology. In a - C_{28} , the molecules are mostly three- and four-fold coordinated, similar to C atoms in amorphous systems. They are connected by single bonds, whose average length (1.55 \AA) is close to the nearest neighbor bond distance in diamond [see Fig. 2(b)]. We classified the reactivity of different fullerene sites [A , B and C , see Fig. 1(a)] in a - C_{28} , according to their probability of forming bonds with other fullerenes and found that A sites are the most reactive sites, followed by C and B sites. Their probability of bond forma-

tion are 0.35, 0.15 and 0.08, respectively. These results agree well with the corresponding reactivities found for a C_{28} thin film grown on a semiconducting substrate,¹¹ where the bonding probability of A , C and B sites were 0.37, 0.11 and 0.04, respectively.

The particle density of the system is very low, 0.9 g cm^{-3} , in contrast to the density of graphite and diamond, which are 2.27 and 3.5 g cm^{-3} , respectively. This particle density agrees with that of the C_{28} 's film grown on a semiconducting surface¹¹ ($\approx 1 \text{ g cm}^{-3}$) and with that determined experimentally for films obtained by LECBD (Ref. 5) ($0.8 \pm 0.2 \text{ g cm}^{-3}$).

The percentage of fourfold coordinated C atoms is small in a - C_{28} , the average atomic coordination being 3.14, as in hyperdiamond. Figure 2(a) shows the particle-particle correlation function $g_{CC}(r)$ including all C atoms (solid line), compared to a correlation function including only atoms which are taking part in *intra*-cluster bonds ($g_{CC}^{intra}(r)$, dashed line) but not in *inter*-cluster bonds. The two correlation functions have been obtained by convoluting the data with a Gaussian corresponding to a maximum wave vector (q_{max}) of 50 \AA^{-1} , according to the procedure of Etherington *et al.*²⁵ The shape of $g_{CC}(r)$ with its several peaks up to distances of 6 \AA clearly indicates that the system is not an ordinary amorphous carbon solid, but it is composed of more complex units. The similarity of $g_{CC}(r)$ and $g_{CC}^{intra}(r)$ shows again that particle-particle correlations are largely determined by the bonds within the units composing the system. The first peaks of $g_{CC}(r)$ and $g_{CC}^{intra}(r)$ are shown again in Fig. 2(b), together with the first peak of the correlation function for all atoms taking part in *inter*-cluster bonds ($g_{CC}^{inter}(r)$). In Fig. 2(b) the data have been convoluted with a Gaussian corresponding to $q_{max} = 90 \text{ \AA}^{-1}$, in order to make visible the shoulders in $g_{CC}^{intra}(r)$ and $g_{CC}(r)$ after the first sharp peak, which are washed out when using convolutions with smaller wave vectors. It is seen that the average *inter*-cluster bond length is close to first-neighbor distances in diamond, as mentioned earlier; *intra*-cluster bond lengths are in general smaller (the first peak of $g_{CC}^{intra}(r)$ is centered at 1.44 \AA), with a small proportion of *intra*-cluster bonds corresponding to diamond-bond lengths. The angular distribution of atoms belonging to the same cluster is shown in Fig. 3(a) and that of atoms forming a *inter*-cluster bonds in Fig. 3(b). This is a broad distribution with a peak at about 115 deg. , an angle bigger than the tetrahedral bond angle, indicating that the four-fold coordinated sites involved in *inter*-cluster bonds are distorted sp^3 sites. Similarly, carbon sites involved in *intra*-cluster bonds are highly distorted sp^2 sites, with bond angles as small as 110 deg.

In Table II we compare the stability and structural properties of a - C_{28} with those of ordered C_{28} solids: hyperdiamond, 2D-hypergraphite, 2D- and close-hexagonal and a clathrate solid. These lattices are illustrated in Fig. 4. The cohesive energy of each ordered solid was computed after optimizing both the volume and the atomic positions. In the case of the clathrate, MD runs at 500 K were performed to allow for a local readjustment of the bonds between fullerenes, initially prepared with random orientations.

The most stable structure is hyperdiamond, which is 0.08

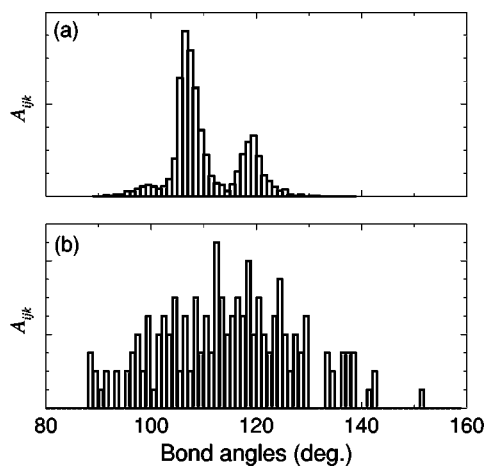


FIG. 3. Bar-chart graph of the angular distributions (A_{ijk}) of carbon sites in amorphous C_{28} . The upper panel (a) shows the distribution of $i-j-k$ sites with j involved in bonding to fullerenes and i and k belonging to different clusters. The lower panel shows the distribution of $i-j-k$ sites with i, j and k belonging to the same cluster.

eV and 0.1 eV lower in energy than hypergraphite and $a-C_{28}$, respectively. Interestingly, the energy of $a-C_{28}$ is degenerate with that of a 2D-hexagonal lattice, where C_{28} molecules have different coordination properties: all of them are six-fold coordinated, as opposed to an average coordination of 3.45 in $a-C_{28}$. The disordered $a-C_{28}$ and ordered 2D-hexagonal solid are slightly more stable (0.01–0.02 eV) than clathrate and close hexagonal lattices. We note that the particle density of the clathrate structure is 30% larger than that of $a-C_{28}$, with 88% of the sites involved in bond formations, as opposed to 52% in $a-C_{28}$. This indicates that C_{28} molecules can be packed in several different ways to form a condensed phase. Solids can be built which have different bonding characteristics and volume occupancy, yet having similar cohesive energies.

The electronic properties of ordered and disordered C_{28} structures also show important differences. Hyperdiamond is an insulator with a gap of about 2 eV, whereas all other structures are gapless solids. The electronic density of states (EDOS) of $a-C_{28}$ is shown in Fig. 5, where it is compared with those of a C_{28} monomer and dimer. Two cases have been considered for the monomer: the optimized geometry of the free cluster, which is Jahn-Teller distorted and the perfect dodecahedron, which has T_d symmetry. The EDOS of the Jahn-Teller distorted monomer, the dimer and $a-C_{28}$ are

TABLE II. Cohesive energy (E_{coh}), average coordination of C_{28} molecules (C_{28} coord.), average atomic coordination (atomic coord.) and average intercluster bond lengths (B.L.) in several ordered and disordered solids composed of C_{28} molecules.

Structure	E_{coh}	C_{28} Coord.	Atomic Coord.	B.L.
Hyperdiamond	6.61	4	3.14	1.52
2D-Graphite	6.52	3	3.11	1.50
2D-hexagonal	6.51	6	3.21	1.51
Closed-hexagonal	6.49	6	3.21	1.51
clathrate	6.48	3.74	3.14	1.51 (1.57)
$a-C_{28}$	6.51	3.45	3.14	1.55

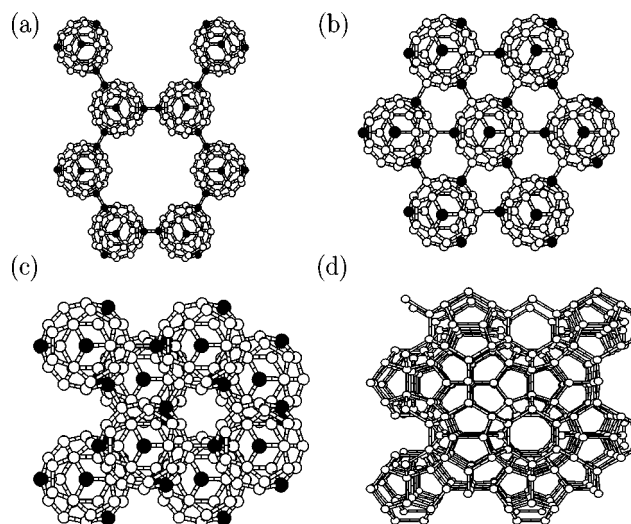


FIG. 4. Ordered solids composed of C_{28} molecules: Hypergraphite (a), 2D-hexagonal (b), closed-hexagonal (c) and a clathrate solid (d), where the centers of mass of the molecule occupy the lattice site of a two-dimensional graphite lattice, a two-dimensional hexagonal lattice, a three-dimensional closed-hexagonal lattice and a three-dimensional clathrate solid with 46 molecules per unit cell, respectively. Black spheres indicate A sites. In the case of the clathrate solid we only indicated the position of the centers of mass of the molecules.

similar, confirming that also from the electronic structure point of view the C_{28} cluster act as the building block of the disordered solid. The EDOS of $a-C_{28}$ has a deep dip in correspondence of the Fermi level, however no clear gap can be identified. Calculations of the electrical conductivity would be required, in order to establish whether the system is metallic.

While the Jahn-Teller distorted monomer is the building block of $a-C_{28}$, our calculation, in agreement with previous

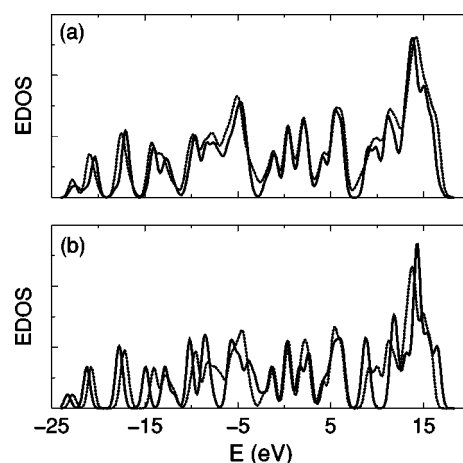


FIG. 5. Electronic density of states of amorphous C_{28} (a, solid line) a C_{28} dimer (a, dotted line), the Jahn-Teller distorted monomer (b, dotted line) and the monomer in a T_d -symmetrical geometry (b, solid line). The data have been broadened with a Gaussian smearing of 0.5 eV. The highest occupied orbital of the symmetric monomer, at 2.59 eV, is three-fold degenerate and occupied by four electrons; that of the asymmetric dimer, at 2.33 eV, is nondegenerate and separated by about 0.25 eV from the lowest unoccupied orbital. The highest occupied orbitals of amorphous C_{28} and the C_{28} dimer are at 2.36 and 2.29 eV, respectively. In our calculations, the dimer has a small gap of 0.1 eV and amorphous C_{28} is a gapless solid.

results,⁹ suggest that the C_{28} cluster with T_d symmetry is the building block of hyperdiamond. In order to have a qualitative understanding of the opening of a gap in hyperdiamond, we consider the electronic properties of $C_{28}H_4$, where H atoms are bonded to A sites. In this molecule the C_{28} unit has bonding and hybridization properties similar to those of one C_{28} in hyperdiamond.⁹ In a similar way, an analogy can be traced between the bonding and hybridization properties of carbon in CH_4 and in diamond. The highest occupied molecular orbital (HOMO) of C_{28} is three-fold degenerate, i.e., it can accommodate six electrons, and occupied by four electrons. The lowest unoccupied orbital (LUMO) is nondegenerate and separated in energy from the following orbital by a gap of about 1.6 eV. When forming $C_{28}H_4$, the HOMO and LUMO of C_{28} are completely filled and thus a closed shell molecular orbital structure is achieved, where the occupied and empty states are separated by a large gap.

IV. CONCLUSIONS

We have performed tight-binding molecular dynamics simulations mimicking the gas-phase growth of a disordered C_{28} solid (a - C_{28}), and compared the structural and electronic properties of this disordered system with those of crystalline forms of C_{28} . We have shown that for certain growth conditions (i.e., in a certain collision energy regime), an amorphous system is formed, composed of undamaged C_{28} molecules. Our findings point towards the possibility of synthesizing new covalently bonded fullerite materials. In a - C_{28} , the molecules are mostly three- and four-fold coordinated, similar to C atoms in amorphous systems. However the C_{28} clusters show more bonding flexibility than C atoms, since they can be six-fold coordinated building blocks of hexagonal solids which are as stable as a - C_{28} and 2D-hypergraphite. Our results for the structural and bonding properties of a - C_{28} agree well with those for a thin film of C_{28} molecules deposited on a nonmetallic substrate,¹¹ and suggest that the films obtained experimentally by LECBD (Ref. 5) are not diamond-like systems but rather nanostructured materials composed of cages. Finally, we note that collision computer experiments involving C_{24} 's gave remarkably different results from those performed with C_{28} 's, indicating that the formation of an amorphous system composed of C_{24} fullerenes as building blocks is very unlikely.

ACKNOWLEDGMENTS

Part of this work was done as part of the PATP (Parallel Applications Technology Program) joint project between the EPFL and Cray Research. Support is also acknowledged from the Swiss NSF (G.G.) and the United States DOE (J.K.).

- ¹ See, e.g., R. F. Service, *Science* **271**, 920 (1996); G. E. Scuseria *ibid.* **271**, 942 (1996).
- ² See, e.g., *Science and Technology of Fullerene Materials*, MRS Symposia Proceedings No. 359, edited by P. Bernier *et al.* (Materials Research Society, Pittsburgh, 1995); G. Benedek and L. Colombo, *Mater. Sci. Forum* **232**, 247 (1996).
- ³ H. W. Kroto, J. R. Heath, S. C. O'Brien, R. F. Curl, and R. E. Smalley, *Nature (London)* **318**, 1744 (1985).
- ⁴ For a review see, e.g., C. A. Mirkin and W. B. Caldwell, *Tetrahedron* **52**, 5113 (1996).
- ⁵ V. Paillard *et al.*, *Phys. Rev. Lett.* **71**, 4170 (1993); *Phys. Rev. B* **49**, 11433 (1994).
- ⁶ P. Melinon *et al.*, *Carbon* **32**, 1011 (1994); V. Paillard *et al.*, *Nanostruct. Mater.* **4**, 759 (1994).
- ⁷ G. B. Adams, O. F. Sankey, J. B. Page, and M. O'Keeffe, *Chem. Phys.* **176**, 61 (1993).
- ⁸ D. M. Bylander and L. Kleinman, *Phys. Rev. B* **47**, 10967 (1993).
- ⁹ E. Kaxiras, L. M. Zeger, A. Antonelli, and Y-m Juan, *Phys. Rev. B* **49**, 8446 (1994).
- ¹⁰ L. M. Zeger, Y-m Juan, E. Kaxiras, and A. Antonelli, *Phys. Rev. B* **52**, 2125 (1995).
- ¹¹ A. Canning, G. Galli, and J. Kim, *Phys. Rev. Lett.* **78**, 4442 (1997).
- ¹² Y. Achiba *et al.*, *Mater. Sci. Eng. B* **19**, 14 (1993).
- ¹³ T. Guo *et al.*, *Science* **257**, 1661 (1992).
- ¹⁴ W. H. Kroto, *Nature (London)* **359**, 529 (1987).
- ¹⁵ P. Milani *et al.*, *J. Appl. Phys.* (to be published).
- ¹⁶ C. Xu *et al.*, *J. Phys.: Condens. Matter* **4**, 6047 (1992).
- ¹⁷ J. Kim, F. Mauri, and G. Galli, *Phys. Rev. B* **52**, 1640 (1995).
- ¹⁸ For a review see, e.g., G. Galli, *Curr. Opinion Solid State Mater. Sci.* **1**, 6, 864 (1996).
- ¹⁹ B. L. Zhang, C. Z. Wang, K. M. Ho, C. H. Xu, and C. T. Chan, *J. Chem. Phys.* **97**, 5007 (1992).
- ²⁰ For a review see, e.g., G. Galli and A. Pasquarello, in *Computer Simulation in Chemical Physics*, edited by M. P. Allen and D. J. Tildesley (Kluwer, Dordrecht, 1993), p. 261; M. C. Payne, M. P. Teter, D. C. Allan, T. A. Arias, and J. D. Joannopoulos, *Rev. Mod. Phys.* **64**, 1045 (1993).
- ²¹ N. Troullier and J. Martins, *Phys. Rev. B* **43**, 1993 (1991).
- ²² M. R. Pederson and N. Laouini, *Phys. Rev. B* **48**, 2733 (1993); K. Jackson, E. Kaxiras, and M. R. Pederson, *ibid.* **48**, 17556 (1993); *J. Phys. Chem.* **98**, 7805 (1994).
- ²³ S. Nosé, *Mol. Phys.* **52**, 255 (1984); W. Hoover, *Phys. Rev. A* **31**, 1695 (1985).
- ²⁴ See, e.g., *Computer Simulation of Liquids*, edited by M. P. Allen and D. J. Tildesley (Oxford Science, Oxford, 1989), p. 232.
- ²⁵ G. Etherington *et al.*, *J. Non-Cryst. Solids* **48**, 265 (1982).